Ceramics International 46 (2020) 6038–6045

Contents lists available at ScienceDirect

Ceramics International

journal homepage: www.elsevier.com/locate/ceramint

Laser surface modification of porous yttria stabilized zirconia against CMAS degradation

S. Bakkar[a], M.V. Pantawane[a], J.J. Gu[a], A. Ghoshal[b], M. Walock[b], M. Murugan[b], M.L. Young[a], N. Dahotre[a], D. Berman[a], S.M. Aouadi[a,*]

[a] Department of Materials Science and Engineering, University of North Texas, Denton, TX, 76203, USA
[b] U.S. Army Futures Command, Aberdeen Proving Ground, MD, 21005, USA

ARTICLE INFO

Keywords:
Freeze-casting
YSZ
Laser processing
Porous ceramics

ABSTRACT

Here, we present a new combined freeze-casting and laser processing method for the design of yttria-stabilized zirconia (YSZ) based thermal-barrier coatings. YSZ ceramics with unidirectionally-aligned pore channels were created using the freeze-casting method. After sintering, top view and cross-sectional scanning electron microscopy (SEM) revealed the structural features of the preform, which exhibits a 74 ± 2% volume fraction of porosity and an average pore channel size of 30 ± 3 μm. The measured thermal conductivity of this porous structure was 0.27 ± 0.02 W/(m K), which is eight times lower than that of reported values for dense YSZ. Though high porosity is beneficial both from a structural and thermal response perspective, the open porosity could potentially be an issue from an application stand-point when evaluating the resistance of materials to calcium–magnesium–aluminum–silicon oxide (CMAS) attack. CMAS attack, which can originate from deposits of molten sand, ash, and dust, is one of the major causes of thermal barrier coating failure. Therefore, the surface of the porous samples was modified using a laser process to create a barrier to CMAS infiltration. SEM micrographs aided in determining the optimum laser parameters required to fully seal the surface using a laser treatment. The performance of the original porous and surface-modified YSZ was compared by conducting CMAS infiltration studies. Laser modification was shown to be a viable technique to significantly reduce CMAS infiltration in porous thermal barrier coatings.

1. Introduction

Yttria-stabilized zirconia (YSZ) [1] is one of the most extensively studied ceramics (studied for over five decades) due to its superior structural stability, chemical inertness, hardness, biocompatibility, and its relatively high thermal resistivity, thermal expansion coefficient, and fracture toughness [2–5]. As a result, YSZ has been widely used in several applications that include thermal barrier coatings (TBCs) in gas turbine engines, refractories in jet engines, dental implants, and, more recently, solid oxide fuel cells and non-metallic knife blades [2–5]. Compared with all potential TBC materials, YSZ was found to be the most successful topcoat ceramic materials due to its low thermal conductivity attributed to its high concentration of point defects, its low relative density, its ability to relax stress caused by incompatibility in terms of coefficient of thermal expansion, and strain tolerance [2]. Additional tuning of the YSZ properties is achieved through the introduction of porosity, which further decreases the thermal conductivity of the materials and increases their adaptability to thermal stresses. The introduction of porosity in YSZ ceramics is usually achieved using methods such as gel-casting, slip-casting, direct foaming, starch consolidation, electrophoretic deposition, template-based sintering, and freeze-casting [6–8].

The thermal and mechanical properties of porous YSZ make it attractive for its use as a TBC. A TBC typically consists of a three-layer coating, which is applied to the surface of a metallic underlayer, such as nickel-based superalloy, by either electron beam physical vapor deposition (EB-PVD) [9] or air plasma spray (APS) [10]. The three-layer coating consists of a YSZ top-coat, an intermediate thermally-grown oxide layer, and a metallic underlayer. The YSZ layer is ~150–250 μm thick and is highly porous. Porosity is an inherent property of both deposition processes. EB-PVD leads to a columnar structure with an average column diameter of ~ 2–4 μm near the substrate that increases to about 10–20 μm towards the air-film interface. The intercolumnar gap is the largest (~1–2 μm) near the air-film interface. APS produces closed pores that are non-directional. Porosity is crucial in the design of TBCs since it reduces their thermal conductivity and enhances adhesion

* Corresponding author.
E-mail address: samir.aouadi@unt.edu (S.M. Aouadi).

https://doi.org/10.1016/j.ceramint.2019.11.061
Received 6 September 2019; Received in revised form 4 November 2019; Accepted 7 November 2019
Available online 20 November 2019

to substrates via stress accommodation. Porosity is, however, detrimental to coating longevity, since it provides a pathway for an accelerated CMAS infiltration and to oxygen diffusion [11].

Mitigation of CMAS attack has recently become a priority for jet engine manufacturers since TBCs are prone to catastrophic failure due to the molten deposits from sand, ash, and dust, which form glassy melts on the coatings. These melts infiltrate the open pores of the TBC structures and react with YSZ thereby resulting in the dissolution of the coating [12]. Thus, CMAS infiltration leads to premature coating failure and significantly reduces the lifespan of engine components [10,13–15]. Degradation of YSZ-based TBCs due to the infiltration of molten salts becomes even more pronounced as the in-service temperature of current aerospace engines is increased to improve efficiency. Researchers are currently investigating various methods to develop new coating designs to mitigate CMAS attack while maintaining the important required protective properties, which include erosion resistance, strain tolerance, and oxidation resistance under the harsh environment of a combustion engine [10].

In this study, we focus on understanding the effect of surface laser processing on free-standing porous YSZ structures produced by freeze-casting [8,16], thus creating an impermeable surface, to reduce CMAS infiltration. Impermeable surfaces consist of protective layers that inhibit liquid CMAS from infiltrating or reacting with the TBC during operation. These layers are typically composed of oxide or metallic surfaces that are dense and nonporous [14]. Freeze-casting is a promising fabrication method that is widely used to synthesize porous materials in areas that pertain to medicine, bioengineering, and energy harvesting and storage [17,18]. It is a technique that is used to cast unidirectionally channeled YSZ structures with controlled porosity. The freeze-casting method, combined with surface laser processing, was selected for two main reasons:

- This method is used as a model system to study and understand the effect of surface modifications on CMAS infiltration without concern for coating adhesion. This technique may also be tested in the future for growing coatings on superalloy substrates.
- The approach enables the formation of a two-layer system that has a low thermal conductivity resulting from high porosity of the freeze-casting method and a laser processed smooth/dense layer that is intended to inhibit CMAS infiltration.

The laser parameters were optimized to modify the surface of the freeze-cast YSZ to form a smooth and dense impermeable layer over the porous thermally-resistant bulk sample. Untreated and treated YSZ surfaces were tested for their resistance to CMAS infiltration. Samples in the various stages of processing were analyzed using X-ray diffraction (XRD), scanning electron microscopy (SEM), and energy dispersive spectroscopy (EDS).

2. Experimental details

2.1. Materials

Porous YSZ samples were created using the following items: yttria-stabilized zirconia powder with a particle size of 0.8 μm (ZrO_2 – 13.5 wt % Y_2O_3, 1 wt% HfO_2, 99.9% purity, SkySpring Nanomaterials Inc., Houston, TX), tert-butyl alcohol (TBA, ≥ 99.0% purity, Sigma- Aldrich Co., St. Louis, MO, USA), and polyvinyl alcohol (PVA, ≥ 99.0% purity, Sigma- Aldrich Co., St. Louis, MO, USA).

2.2. Freeze-casting processing

To create porous YSZ samples, a slurry containing the items described above was prepared with the yttria-stabilized zirconia powder, TBA as a solvent with solid loading (10–40 vol%), and PVA as a binder [19]. The slurry solution consisted of a mixture of 58 wt% YSZ, 40 wt% TBA, and 2 wt% PVA. After mixing by magnet stirring for 3 h, the slurry was poured into a cylindrical polymer mold equipped with a copper plate on the bottom and immersed in liquid nitrogen (−196 °C) for 20–60 min to create unidirectionally-aligned pore channels (Fig. 1). After solidification, the frozen solvent was sublimated using a freeze dryer (LABCONCO Corporation, FreeZone 4.5 plus, Kansas City, MO, USA) in a vacuum (pressure of 0.055 mbar) at −86 °C for 24 h. After sublimation, the YSZ sample was sintered in air at 1450 °C for 2 h at a rate of 8 °C/min.

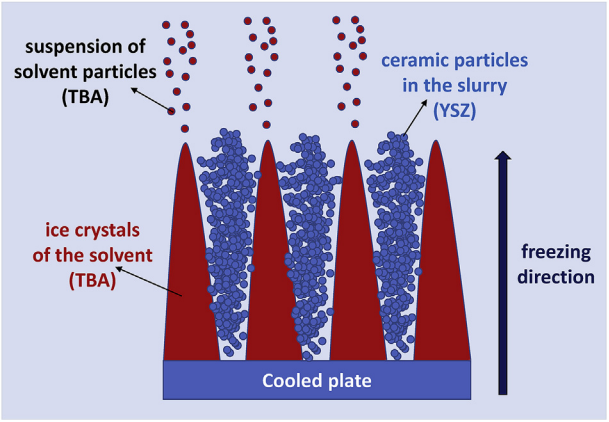

Fig. 1. Schematic diagram illustrating the freeze-casting process to create unidirectionally-aligned pore structures in YSZ-based ceramics.

2.3. Laser processing

Laser surface modification was performed using a continuous wave (CW) Nd:YAG laser system (1.064 μm wavelength) equipped with a Yb fiber optic beam delivery system (Ytterbium Laser System YLS-3000). The laser processing parameters are listed in Table 1. The parameters include laser power, scanning speed, fill spacing (distance between subsequent laser tracks), angle of incidence (measured with respect to laser beam), and laser fluence.

2.4. CMAS testing

After surface modification by laser processing, CMAS testing was carried out using a AFRL 02 CMAS powder (PTI Powder Technology Inc., Arden Hills, MN, USA) with the following composition (in wt.%): 34% Quartz, 30% Gypsum, 17% Aplite, 14% Dolomite, and 5% Salt (NaCl) (99.99% purity). The test was performed before and after laser treatment by melting 0.1 g of the CMAS powder on the surface of the samples in a furnace at 1250 °C for 10 h.

Table 1
Laser parameters employed to optimize the laser surface modification of the free-standing porous YSZ structures.

Power (W)	Scanning speed (mm/s)	Fill spacing (mm)	Angle of laser incidence (°)	Laser Fluence (J/mm^2)
300	100	0.20	90	6.4
200	200	0.20	90	2.1
200	150	0.20	90	2.8
200	100	0.20	90	4.3
100	70	0.20	90	3.0
100	20	0.20	90	10.6
100	20	0.20	60	9.2
150	20	0.25	60	13.8
150	20	0.20	60	13.8
150	20	0.15	60	13.8
150	20	0.10	60	13.8

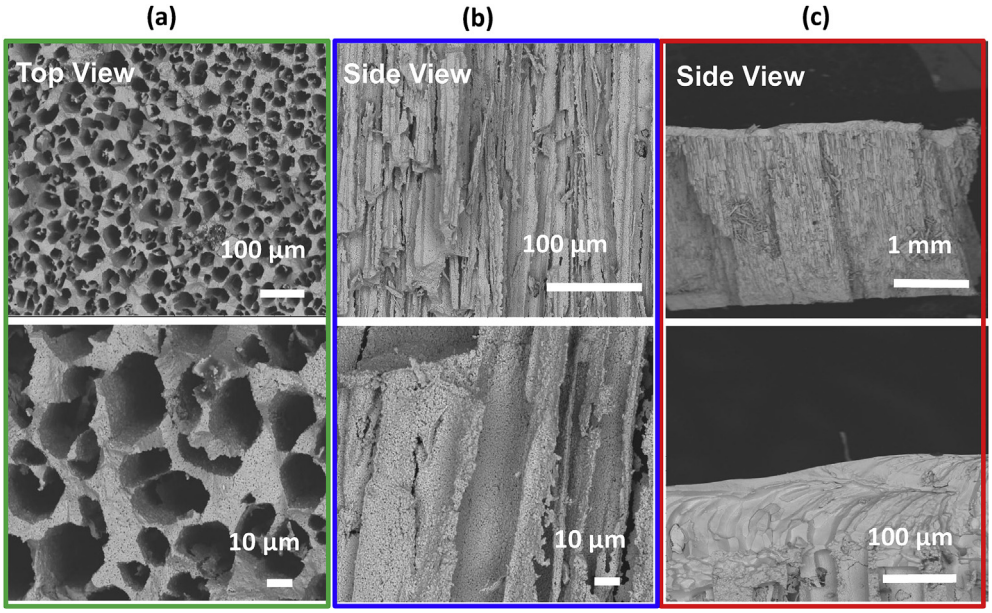

Fig. 2. (a) Top view and (b) cross-sectional SEM micrographs of YSZ structures with unidirectionally-aligned pore channels, which occur at a freeze-casting temperature of −196 °C (c) the thickness of glazing layer after laser-treatment (100w-20mm/s-0.2 mm).

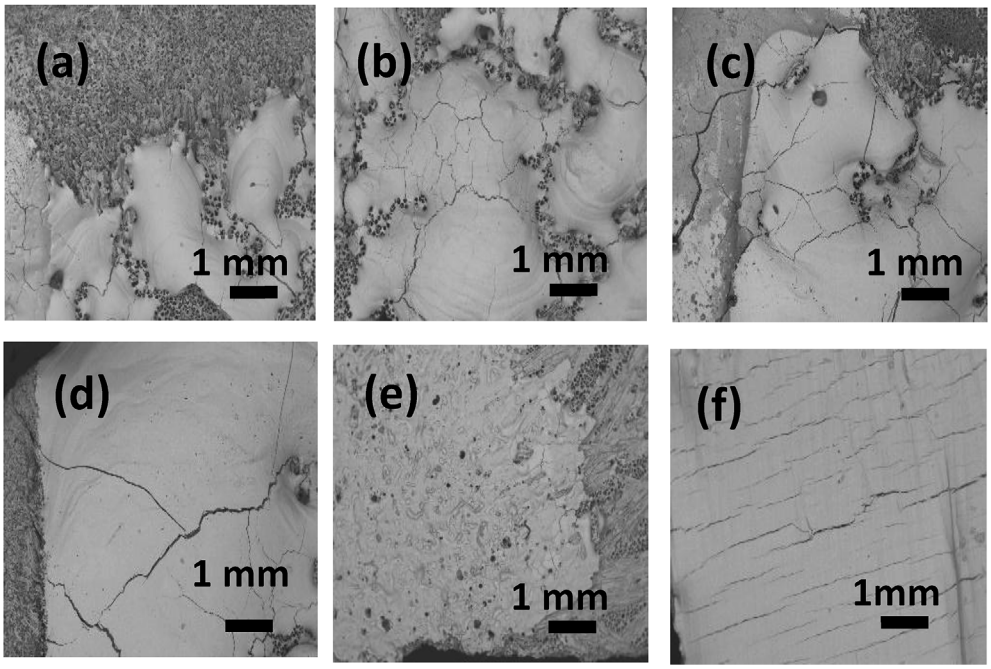

Fig. 3. (I) Top view of porous YSZ produced by freeze-casting and whose surface is laser treated with the sample perpendicular (90°) with respect to the laser beam using the following power (W) - scanning speed (mm/s) - filling space (mm): (a) 200-200-0.2 (b) 200-150-0.2 (c) 200-100-0.2 (d) 300-100-0.2 (e) 100-70-0.2 (f) 100-20-0.2. (II) Top view of porous YSZ produced by freeze-casting and whose surface is laser treated with the sample perpendicular (90°) and (60°) with respect to the laser beam using the following power (W) - scanning speed (mm/s) - filling space (mm) respectively: (a) 100-20-0.2-0° and (b) 100-20-0.2–60°.

2.5. Characterization

X-ray diffraction (XRD) measurements were collected using a Rigaku Ultima III with a Cu Kα radiation source at a scanning rate of 3°/min. XRD was used to evaluate the phase and composition evolution of the porous YSZ samples during the various processing and CMAS testing steps. An FEI Nova 200 Nanolab dual-beam focused ion beam (FIB)/scanning electron microscope (FESEM), with Pt GIS, Omniprobe Nanomanipulator, EDS and EBSD operated at 30 keV, was used to examine the morphology of the samples and to create elemental maps for selected regions of the coatings before and after CMAS testing. The thermal conductivity measurements were collected using thermal constants analyzer, hot disk TPS 2500 S for samples before and after laser treated.

3. Results and discussion

Fig. 2 shows the SEM micrographs of porous YSZ ceramics produced using the freeze-casting technique. The top view micrographs (Fig. 2(a)) revealed a porous structure with vertical pores with a diameter of 30 ± 10 µm and wall thickness (inter-porosity spacing) of 20 ± 10 µm. The pores displayed a nearly hexagonally-shaped cavity because of using very low freezing temperature of −196 °C and because of the crystallization characteristics of the TBA at this temperature (these are the only conditions that allow us to create such structures) [8]. The cross-sectional view in Fig. 2(b) confirmed the formation of unidirectional channels of pores that were found to be consistent with the structure reported by Hu et al. [8] for similar processing conditions. They claimed that solidification velocity increases with a decrease in freezing temperature, which results in a decrease in prism spacing and

thus pore channel size. The porous YSZ samples exhibited relatively homogeneous lamellar microstructures with long-range channels. The high magnification image highlighted in Fig. 2(b) indicated that the wall of the YSZ structure was textured and included finer porosity as a result of the sintering of nanoscale powders. The porosity of the overall structure was estimated to be 74 ± 2% from cross-sectional SEM micrographs. The thickness of the glazing layer ranged from 0.1 to 0.3 mm depending on the processing parameters, as was determined from cross-sectional SEM micrographs as a function of laser processing conditions Fig. 2(c).

Initially, the glazed surfaces were obtained by scanning the surface of the freeze-cast sample with a laser beam normal to the surface. Fig. 3 presents a set of SEM micrographs showing the top view of laser-treated porous YSZ structures for various laser parameters (power, scanning speed, and filling space), which were laser treated with the sample perpendicular to the laser beam (90°). As illustrated in Fig. 3 (a-e), samples treated with a laser fluence < 7 J/mm^2 with scanning speed $>$ 70 mm/s formed patches of melt regions scattered over the porous structure. It is clear that samples treated at higher scanning speeds resulted in insufficient time for the melt to spread uniformly over the porous surface usually due to the rapid cooling rate. Surface modification with a laser fluence in the 10.6 J/mm^2 range (with scanning speed of 20 mm/s) resulted in the elimination of surface porosity by continuous melt layer formation with a network of fine cracks perpendicular to the surface (Fig. 3 (f)). The crack density and crack width were found to be substantially reduced for samples treated with the larger laser fluence values owing to slower scanning speeds (~20 mm/s). Similar results were reported by Batista et al. [20] who were able to seal the porous surface of YSZ coatings manufactured by APS with either a CO_2 or a Nd:YAG laser. This porosity is also an inherent property of the APS process. Though the samples demonstrated good sealing of the porosity, crack formation was still observed due to thermal stresses induced by the rapid cooling rate involved in laser processing.

In an attempt to reduce the density and the size of the cracks, the angle of the laser beam was tilted at 30° to the platform before laser treating the porous YSZ sample (60° with respect to the laser beam), as depicted in Fig. 4-I. Changing the angle of the laser beam effectively changes the angle of laser incidence on the surface of the YSZ sample and changes the influence of the dynamic and gravitational forces acting on the molten YSZ sample, thus, ultimately changing the surface topography, as shown in Fig. 4-II. Fig. 4-II (a) and (b) show the difference between surfaces that were laser treated at angles 90° and 60° with respect to the laser beam, respectively. This figure suggested that laser processing at an inclined angle resulted in fewer and thinner cracks on the surface of the porous ceramic structures.

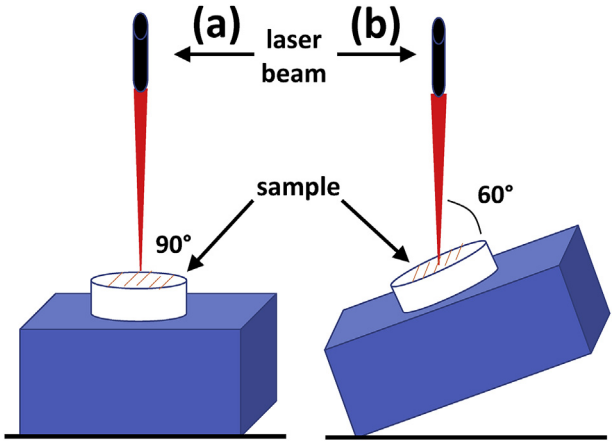

Fig. 4. Schematic diagram of the laser treatment, which was carried out in two configurations, with the sample (a) perpendicular (90°) and (b) at a 60° angle with respect to the laser beam.

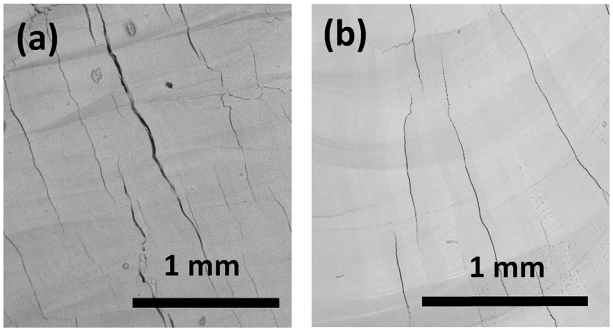

Fig. 4. (*continued*)

The next step consists of investigating the effect of fill spacing on the morphology of the laser modified surfaces. The values for the power, scanning speed, and angle of incidence of the laser beam were selected to be 150 W, 20 mm/s, and 60°, respectively, leading to a laser fluence of (13.8 J/mm^2). Fig. 5 presents the SEM micrographs showing the top view of porous YSZ structures when the filling space was varied in the range between of 0.25 and 0.1 mm. The density of surface cracks was reduced the most for a fill spacing of 0.1 mm. Four different fill spacings (0.1, 0.15, 0.2, 0.25 mm) were utilized to optimize the laser treatment conditions (Fig. 5 (a)–(d)). Investigation of surface topography as a function of processing conditions revealed that the optimum laser scanning conditions were: (i) laser power of 150 W; (ii) scanning speed of 20 mm/s; and, (iii) fill spacing of 0.1 mm. High magnification micrographs, highlighted in Fig. 5, revealed a microstructure with features in the 2–5 μm range, which may be a desirable feature to create a potentially sand-phobic surface. Recently, Kang et al. [15] compared the interaction of CMAS with plasma-sprayed and femtosecond laser ablated YSZ coatings. They concluded that laser-ablated coatings exhibited only a slight decrease in contact angle, contact diameter, droplet height, and droplet volume during a test that lasted for hours suggesting that spreading and penetration of CMAS were both retarded [15].

The room-temperature thermal conductivity of the porous YSZ ceramics (74 ± 2% porosity) along the freezing direction was measured to be 0.27 ± 0.01 W/mK for nano- and micron-size powders. Our measured value is consistent with the value reported by Hu et al. [8] who conducted a systematic study to determine thermal conductivity as a function of porosity. The thermal conductivity is significantly lower than for bulk YSZ (2.18 W/mK [8]). After laser treatment, the thermal conductivity increased from 0.27 ± 0.01 to 0.38 ± 0.01 W/mK. This increase in the thermal conductivity is expected since the laser treatment created a significantly denser top surface.

The laser processed YSZ samples were tested for their resistance to CMAS infiltration. Fig. 6(a) and (b) show top view and cross-sectional SEM micrographs highlighting potential CMAS penetration in (a) untreated and (b) laser-treated bulk samples. The laser scanning conditions of the sample shown in Fig. 6(b) were the optimized and correspond to (i) a laser power of 150 W at 60° with respect to the laser beam, (ii) a scanning speed of 20 mm/s, and, a fill spacing of 0.1 mm. Two different magnifications were selected to highlight different scales of surface features. In the case of the as-cast and untreated sample, CMAS penetrated inside the porous channels. Meanwhile, laser processing of the sample resulted in CMAS forming a smooth layer over an equally smooth laser-modified surface. Fig. 6(c) and (d) illustrates a schematic diagram of the mechanism of CMAS infiltration for untreated and surface-treated samples, respectively. Cracks in the laser-treated samples remained accessible to CMAS penetration indicating the importance of sample uniformity. Similar observations were made for all samples regardless of processing conditions. Cross-sectional SEM and the corresponding EDS elemental mapping for samples synthesized by

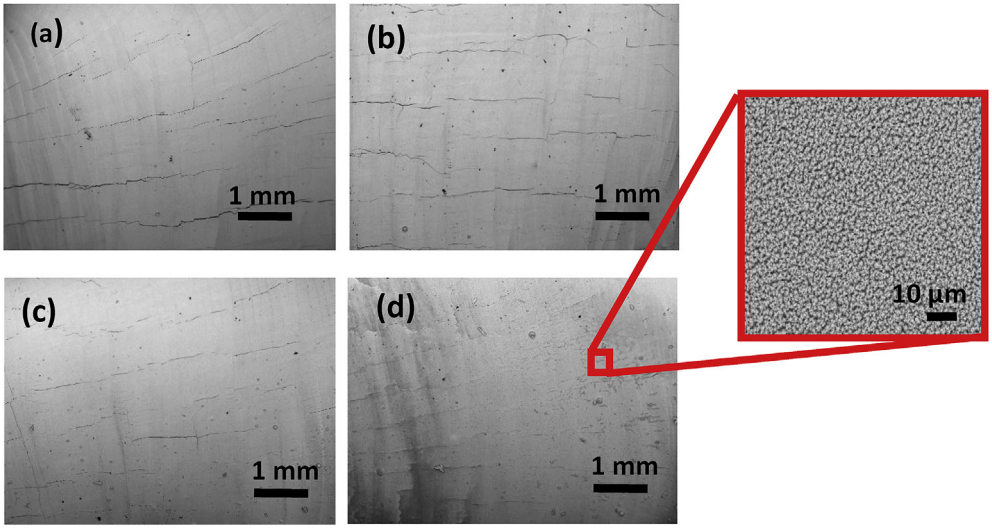

Fig. 5. Top view of porous YSZ produced by freeze-casting and whose surface is laser treated with the sample at a 60° angle with respect to the laser beam using the following power (W) - scanning speed (mm/s) - filling space (mm): (a) 150-20-0.25 (b) 150-20-0.2 (c) 150-20-0.15 and (d) 150-20-0.1.

freeze casting and tested for CMAS infiltration at 1250 °C for 10 h are shown in Fig. 7. Also included in this figure is a table providing the elemental composition in atomic percent measured for the highlighted area using EDS. This figure revealed massive CMAS infiltration in the vertically-aligned pore channels as highlighted by the maps corresponding to Ca, Mg, Al, and Si, which displayed similar profiles. Molten CMAS that rapidly infiltrated YSZ, solidified in the pores after cooling leading to the creation of high internal stresses that will lead to failure of the protective structure. In addition, the molten salt reacted chemically with YSZ to produce new phases or induce phase transitions, as revealed by the XRD data (discussed in a section below), both of which are also detrimental to the lifetime of the TBC [15].

Fig. 8 shows the cross-sectional SEM and the corresponding EDS elemental mapping for a selected laser-treated porous YSZ after CMAS testing. The selected sample's surface was laser-treated at a 60° with respect to the laser beam using a power of 150 W, a scanning speed of 20 mm/s, and a fill spacing of 0.1 mm. This figure revealed that minimal CMAS infiltration occurred only through surface cracks. Fig. 8 also highlights the composition in two areas that correspond to regions below a completely sealed surface (area 1) and cracked surface (area 2). Hence, surface treatment of porous structures is a viable pathway to significantly reduce CMAS-infiltration. Tsai and Hsu [13] reported that laser-glazing of plasma-sprayed YSZ coatings provided a fourfold enhancement in their lifetime in hot corrosion tests using V_2O_5 salt. The infiltration of this salt was reduced by decreasing the density of salt infiltration pathways through the formation of a dense glazed overlayer.

Fig. 9 shows XRD spectra for freeze-cast YSZ samples after sintering at 1450 °C for 2 h in the air (a) for the untreated sample and (b) after surface modification using a laser fluence of 13.8 J/mm^2. These spectra were taken before and after CMAS testing. XRD spectra for the original CMAS powder is also shown as a reference. These spectra suggest that the YSZ samples before and after laser processing consisted of cubic ZrO_2 (c-ZrO_2 - PDF Card No.99-000-0162). The XRD spectra did not change substantially upon laser processing suggesting phase stability upon undergoing the surface treatment. The c-ZrO_2 peaks became sharper after laser processing (peaks with full width at half-maximum values of 0.56 ± 0.02° and 0.22 ± 0.02° before and after laser processing, respectively) suggesting further grain sintering of YSZ crystallites. Similar results, not shown in the figure, were obtained for samples produced using laser processing values > 7 J/mm^2. After CMAS testing, XRD spectra revealed the occurrence of chemical reactions at the solid-liquid interface and the formation of ternary oxides (Ca_2SiO_4, $CaZr_4O_9$, $MgSiO_3$, $ZrSiO_4$). In addition, a small percentage of the YSZ structure underwent a phase change from cubic to monoclinic for both the as-processed and the laser-treated samples. Similar observations were made for YSZ in the t's phase as well. The chemical reactions and phase transformations were attributed to the dissolution and re-

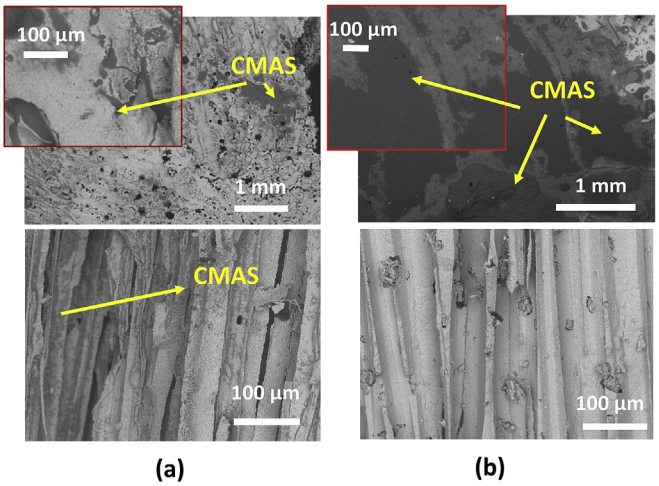

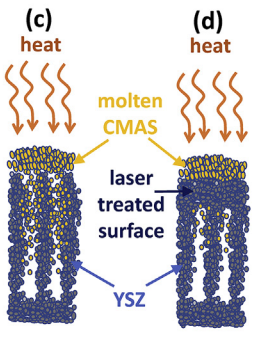

Fig. 6. Top view and cross-sectional SEM micrographs for YSZ ceramics with unidirectionally-aligned pore channels post CMAS testing: (a) as produced and (b) laser-treated 150-20-0.1–60°. Insets in (a) and (b) present higher magnification analysis of the surfaces. Schematic diagram of CMAS test for (a) untreated and (b) treated YSZ surfaces, respectively.

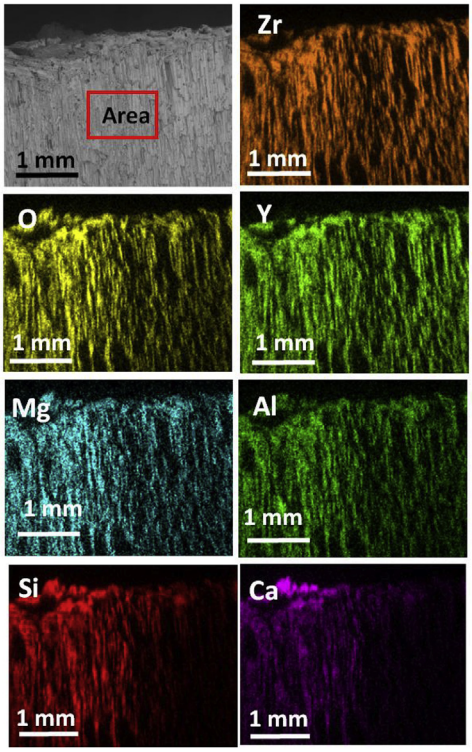

Area	
Element	Atomic %
O	72.01
Na	1.05
Mg	0.71
Al	0.56
Si	7.02
Ca	2.53
Zr	14.16
Hf	0.17
Y	1.78
Total	100.00

Fig. 7. Cross-sectional SEM micrograph and corresponding EDS elemental maps of the untreated YSZ freeze-cast sample with unidirectionally-aligned pore channels and post CMAS testing.

precipitation of YSZ grains in CMAS melt [21]. During dissolution, both the Zr^{4+} and Y^{3+} cations migrate to the molten CMAS. The diffusion of Zr^{4+} cations occurs faster than for Y^{3+} and are able to quickly saturate the glassy CMAS phase. Once the solubility limit of Zr^{4+} in the glassy-CMAS is reached, the Y-deficient ZrO_2 grains re-precipitate [22]. The decrease in Y-content in ZrO_2 causes a martensitic phase transformation to m-ZrO_2 upon cooling. The CMAS-TBC interaction is more severe in the top region of the TBC and may be detrimental to the durability of TBCs (delamination cracking) [23].

Laser-treated porous structures starting with nanoscale-size YSZ particles were also produced to compare with CMAS infiltration as a function of particle size. The selected sample's surface was laser-treated using a power of 150 W, a scanning speed of 20 mm/s, a fill spacing of 0.1 mm at 60° with respect to the laser beam, i.e. the optimum processing conditions, in terms of resistance to CMAS attack based on samples created with micron-scale particles. Fig. 10 shows top view and cross-sectional SEM micrographs for samples produced with an average particle size of 20 ± 3 nm. Top view micrographs demonstrated the formation of a porous structure. The cross-sectional micrographs indicated the formation of unidirectionally-aligned pore channels that have the same size as the ones created with a particle of 800 nm. The only difference is that the columns are denser, as expected, due to the initial smaller particle size. CMAS infiltration tests provided similar results for samples produced with nano- and micron-size YSZ powders.

4. Conclusions

Here, we introduced a new combined freeze-casting and laser processing approach to design highly porous YSZ structures with enhanced resistance to CMAS attack. Porous yttria-stabilized zirconia (YSZ) samples were produced by freezing YSZ/tert-butyl alcohol (TBA)/polyvinyl alcohol (PVA) slurry under a freezing temperature of −196 °C. The frozen slurry was sublimated using a freeze-drying system in a vacuum (0.055 mbar) at −86 °C and then sintered at 1450 °C for 2 h in air. Scanning electron microscopy studies revealed that the porous ceramic structures consisted of vertically-aligned pore channels with an average diameter of 30 ± 6 μm. The porosity volume fraction was determined to be 74 ± 2%. The thermal conductivity of this structure was 0.27 W/(m K). The surface of the sintered samples was glazed using a laser beam to create a smooth thin overlayer. Laser scanning conditions were optimized to produce a compact overlayer with the lowest defect density. The optimum conditions were determined by comparing top view and cross-sectional SEM micrographs for samples produced using different conditions. A laser power of 150 W at 60° with respect to the laser beam, a scanning speed of 20 mm/s, a filling space of 0.1 mm, resulted in the lowest density of surface cracks. The performance of the as-produced and surface-modified YSZ porous structures was compared by conducting CMAS

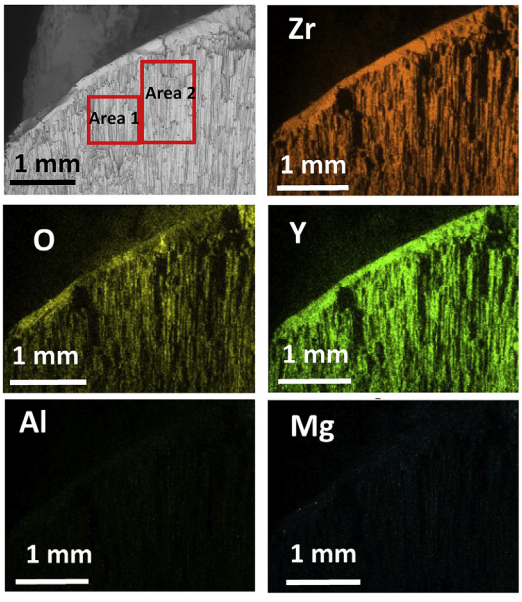

Area 2	
Element	Atomic %
O	72.37
Na	0.37
Mg	0.46
Al	0.35
Si	2.89
Ca	1.10
Y	2.75
Zr	19.51
Hf	0.21
Total	100.00

Area 1	
Element	Atomic %
O	71.85
Y	3.62
Zr	24.31
Hf	0.22
Total	100.00

Fig. 8. Cross-sectional SEM micrograph and corresponding EDS elemental maps of the YSZ freeze-cast sample with unidirectionally-aligned pore channels and post CMAS testing for a laser treated samples (150w-20 mm/s-0.1 mm-30°).

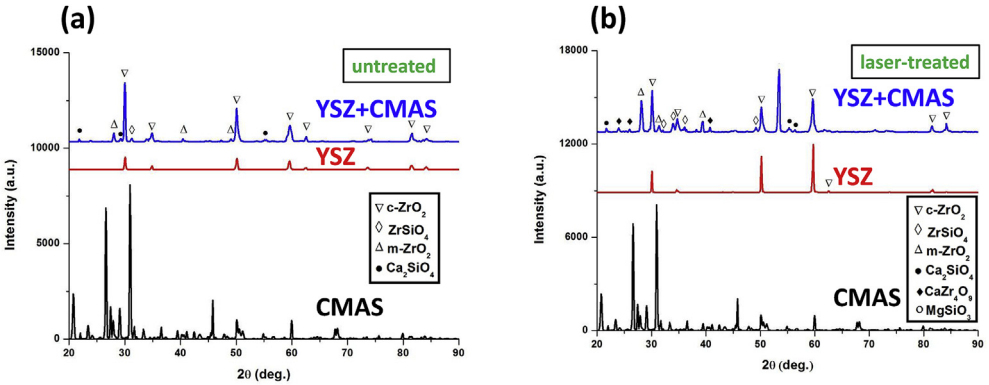

Fig. 9. XRD patterns from (a) as-produced and (b) laser-treated samples of CMAS, YSZ sintered at 1450 °C for 2 h, and YSZ sintered at 1450 °C for 2 h and after CMAS testing.

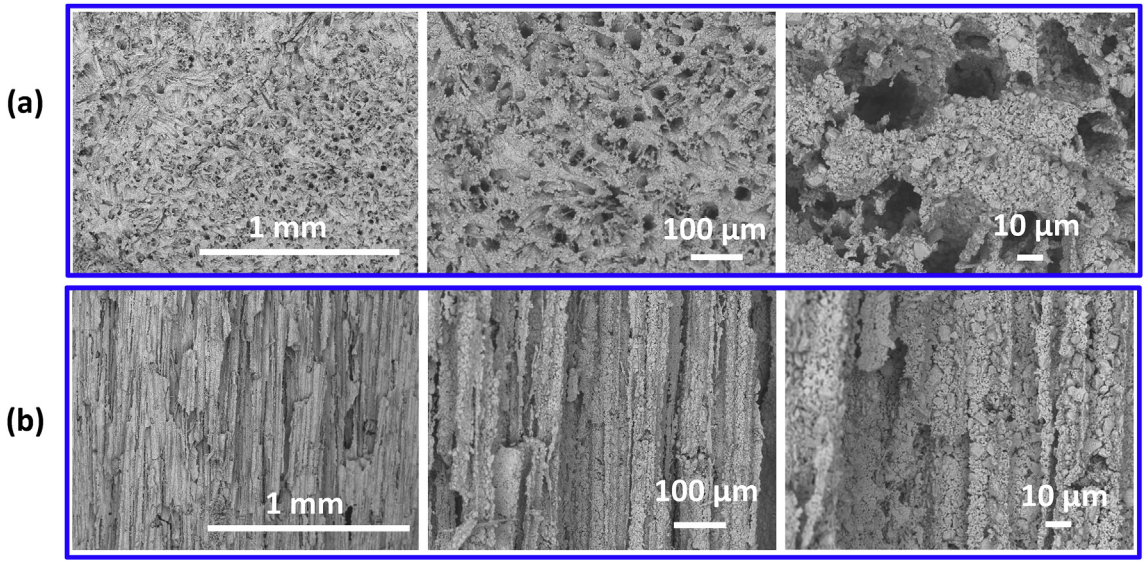

Fig. 10. (a) Top view and (b) cross-sectional SEM micrographs of YSZ structures with unidirectionally-aligned pore channels with particle size 20 nm.

infiltration studies. The key finding of this study was that laser modification was shown to significantly reduce CMAS infiltration. Our results provide a new alternative approach for the synthesis of TBCs which can be adapted for materials beyond YSZ.

Declaration of competing interests

The authors declare that they have no known competing financial interests or personal relationships that could have appeared to influence the work reported in this paper.

Acknowledgments

The authors acknowledge partial funding from the.Army Research Laboratory This work was performed in part at the University of North Texas's Materials Research Facility.

References

[1] B. Butz, R. Schneider, D. Gerthsen, M. Showalter, A. Rosenauer, Decomposition of 8.5 mol.% Y_2O_3-doped zirconia and its contribution to the degradation of ionic conductivity, Acta Mater. 57 (2009) 5480–5490.
[2] D.R. Clarke, S.R. Phillpot, Thermal barrier coatings, Mater. Today 8 (2005) 22–29.
[3] H. Nishihara, M.H. Adanez, W. Att, Current status of zirconia implants in dentistry: preclinical tests, J. Prosthodont. Res. 63 (2019) 1–14.
[4] K.H. Ng, H.A. Rahman, M.R. Somalu, Review: enhancement of composite anode materials for low-temperature solid oxide fuels, Int. J. Hydrogen Energy 44 (2019) 30692–30704 (In Press).
[5] J.J. Gu, S.S. Joshi, Y.-S. Ho, B.W. Wei, T.Y. Hung, Y.Y. Liu, N.B. Dahotre, S.M. Aouadi, Investigation of laser processed YSZ-Al_2O_3-TiC self-healing layers for thermal barrier coatings, Thin Solid Films 688 (2019) 137481.
[6] T. Wu, W. Zhang, B. Yu, J. Chen, A novel electrolyte-electrode interface structure with directional micro-channel fabricated by freeze casting: a minireview, Int. J. Hydrogen Energy 42 (2017) 29900–29910.
[7] R. Liu, C. Wang, Effects of mono-dispersed PMMA micro-balls as pore-forming agent on the properties of porous YSZ ceramics, J. Eur. Ceram. Soc. 33 (2013) 1859–1865.
[8] L. Hu, C.-A. Wang, Y. Huang, C. Sun, S. Lu, Z. Hu, Control of pore channel size during freeze casting of porous YSZ ceramics with unidirectionally aligned channels using different freezing temperatures, J. Europ. Cerm. Soc. 30 (2010) 3389–3396.
[9] A.F. Renteria, B. Saruhan, U. Schulz, H.-J. Raetzer-Scheibe, J. Haug, A. Wiedenmann, Effect of morphology on thermal conductivity of EB-PVD PYSZ TBCs, Surf. Coat. Technol. 201 (2006) 2611–2620.
[10] A. Nieto, M. Walock, A. Ghoshal, D. Zhu, W. Gamble, B. Barnett, M. Murugan, M. Pepi, C. Rowe, R. Pegg, Layered, composite, and doped thermal barrier coatings exposed to sand laden flows within a gas turbine engine: microstructural evolution, mechanical properties, and CMAS deposition, Surf. Coat. Technol. 349 (2018) 1107–1116.
[11] C. Zhao, M. Zhao, M. Shahid, M. Wang, W. Pan, Restrained TGO growth in YSZ/NiCrAlY thermal barrier coatings by modified laser remelting, Surf. Coat. Technol. 309 (2017) 1119–1125.
[12] Z. Xu, L. He, R. Mu, F. Lu, S. He, X. Cao, Thermal cycling behavior of YSZ and $La_2(Zr_{0.7}Ce_{0.3})_2O_7$ as double-ceramic-layer systems EB-PVD TBCs, J. Alloy. Comp. 525 (2012) 87–96.
[13] X. Chen, Calcium-magnesium-alumina-silicate (CMAS) delamination mechanisms in EB-PVD thermal barrier coatings, Surf. Coat. Technol. 200 (2006) 3418–3427.
[14] A.K. Rai, R.S. Bhattacharya, D.E. Wolfe, T.J. Eden, CMAS-resistant thermal barrier coatings, Int. J. Appl. Ceram. Technol. 7 (2010) 662–674.
[15] Y.X. Kang, Y. Bai, G. Q > Du, F.L. Yu, C.G. Bao, Y.T. Wang, F. Ding, High temperature wettability between CMAS and YSZ coating with tailored surface microstructures, Mater. Lett. 229 (2018) 40–43.

[16] Y. Du, N. Hedayat, D. Panthi, H. Ilkhani, B.J. Emley, T. Woodson, Freeze-casting for the fabrication of solid oxide fuel cells: a review, Materialia 1 (2018) 198–210.
[17] T. Fukasawa, M. Ando, T. Ohji, S. Kanzaki, Synthesis of porous ceramics with complex pore structure by freeze-dry processing, J. Am. Ceram. Soc. 84 (2010) 230–232.
[18] T. Fukasawa, Z.Y. Deng, M. Ando, T. Ohji, Y. Goto, Pore structure of porous ceramics synthesized from water-based slurry by freeze-dry process, J. Mater. Sci. 36 (2001) 2523–2527.
[19] S. Deville, Freeze-casting of porous ceramics: a review of current achievements and issues, Adv. Eng. Mater. 10 (3) (2008) 155–169.
[20] C. Batista, A. Portinha, R.M. Rieiro, V. Texeira, C.R. Oliveira, Evaluation of laser-glazed plasma-sprayed thermal barrier coatings under high temperature exposure to molten salts, Surf. Coat. Technol. 200 (2006) 6783–6791.
[21] B. Zhang, W. Song, H. Guo, Wetting, infiltration and interaction behavior of CMAS towards columnar YSZ coatings deposited by plasma spray physical vapor, J. Eur. Ceram. Soc. 38 (2018) 3564–3572.
[22] A.R. Krause, B.S. Senturk, N.P. Padture, $2ZrO_2{\cdot}Y_2O_3$ thermal barrier coatings resistant to degradation by molten CMAS: part II, interactions with sand and fly ash, J. Am. Ceram. Soc. 97 (2014) 3950–3957.
[23] A.R. Krause, H.F. Garces, G. Dwivedi, A.L. Ortiz, S. Sampath, N.P. Padture, Calcia-magnesia-alumino-silicate (CMAS)-induced degradation and failure of air plasma sprayed yttria-stabilized zirconia thermal barrier coatings, Acta Mater. 105 (2016) 355–366.